ISSN NO. 2320-5407

Journal homepage: http://www.journalijar.com

INTERNATIONAL JOURNAL OF ADVANCED RESEARCH

RESEARCH ARTICLE

Analysis of Degree of Asymmetry between Right and Left halves of the Mandible in A sample of Egyptian Individuals

***Yara Qadry[1] BDS, Susan A. Hassan[2]BDS, MDS, PhD, Fahmy A. Mobarak[3] BDS, MDS, PhD**

1. Resident of Oral and Maxillofacial Surgery. Oral and Maxillofacial Surgery Department. Faculty of Dentistry-Alazhar University.
2. Professor of Oral and Maxillofacial Surgery. Oral and Maxillofacial Surgery Department. Faculty of Dentistry-Alazhar University.
3. Professor of Oral and Maxillofacial surgery. Oral and Maxillofacial Surgery Department. Faculty of Oral and Dental Medicine-Cairo University and consultant of Oral and Maxillofacial Surgery at Nasser Institute Hospital.

Manuscript Info

Manuscript History:

Received: 15 May 2014
Final Accepted: 25 June 2014
Published Online: July 2014

Key words:
Stereolithographic (STL)
Reconstruction plate
Facial asymmetry
Computer-assisted surgery (CAS)

****Corresponding Author***

Yara Qadry

Abstract

Mandibular reconstruction is mandatory for patients with mandibular defect. Computer assisted surgery (CAS), enables the surgeon to obtain stereolithographic (STL) model by mirroring the normal side on the affected one for adaptation of reconstruction plate. However, accuracy of adaptation may be influenced by the natural asymmetry of human skull. So this study was conducted to determine the degree of asymmetry between right and left halves of the mandible. The sample consists of 21 facial CT scans of intact mandible for reconstruction of virtual 3D model .For 3D linear and angular measurements; eight points were marked on each half of the mandible. Another nine points were marked on the whole mandible at its bottom view. For 2D measurements, points used for measurements of buccolingual thickness of the mandible were first marked at 3D model, and then measured at the 2D axial cut. These points were taken at three levels, the alveolar bone (Th_a), above mental foramen (Th_b), and the inferior border (Th_c). At each level, three points were taken on each side. Using paired Student's t test to analyze the difference between right and left halves of the mandible we found that there was a non-significant difference between right and left halves at 2D and 3D measurements, except for Th_{b1} (p=0,006) and Th_{c1} (p=0.008). Therefore we concluded that the mirroring tool is a reliable method in virtual reconstruction of the mandible in cases of unilateral mandibular defect with subsequent printing STL model for preoperative adaptation of the reconstruction plate.

Introduction

Partial mandibular resection is often indicated in patients with benign or malignant tumors, osteomyelitis, trauma, osteoradionecrosis, and bisphosphonate-related osteonecrosis of the jaws. The resulting defect deteriorates the patient's anatomy, speech, nutrition, and overall quality of life. Mandibular reconstruction is required for those patients to recover the proper anatomical morphology and function. It can be done with appropriate techniques, such as reconstruction plates, free bone grafts, microvascular free flaps. However, properly contoured reconstruction plates are crucial in the success of the above mentioned reconstruction procedures. (Yamada et al., 2010; Salgueiro and Stevens, 2010)

Intraoperative plate bending requires more extensive surgical exposure, increasing surgical time and potentially increasing blood loss. The resultant plate may be improperly contoured, resulting in asymmetry, disfigurement, malocclusion and exposure of the plate with skin and/or mucosal dehiscence. Moreover, fracture of the reconstruction plate may occur as a result of fatigue caused by repetitive bending in areas of contouring. With the introduction of computer assisted surgery (CAS), the surgeon can virtually simulate the surgical procedure using surgical simulation software. This virtual simulation is used to obtain a stereolithographic (STL) model which is an accurate representation of patient's CT data set. These models could be used to adapt the reconstruction plate preoperatively. (Salgueiro and Stevens, 2010; Pirgousis et al., 2013; Rahimov and Farzaliyev, 2011)

The mirroring tool employed in surgical simulation software, allows the use of the intact side as a template for computational super-imposition on the affected side. Based on facial symmetry principle unilateral defects (traumatic and oncologic) lend themselves well to CAS techniques. A mirror image of the unaffected side can be created and superimposed on the affected area at the mid sagittal plane. Segmenting the deformed portion of a patient's anatomy and replacing it with a mirror image of the opposite side creating 3D model of the affected side which printed as STL model on which the reconstruction plate will be adapted. (Zhao et al., 2012; Edwards, 2010; Markiewicz and Bell, 2011)

Despite of the importance of mirroring tool, some investigators believed that it may influence the accuracy of preoperative virtual planning because of the natural asymmetry of human skull. (Modabber et al., 2013; Lee et al., 2007)

Anthropological studies proved asymmetry of the human body and the skull itself. Scientific investigations included various aspects of asymmetry – determination of the moment of life when it occurs, causes, types, intensification and factors inducing its development, or evaluation of which part of the skull shows more pronounced asymmetry. (Gawlikowska et al., 2007; Bigoni et al., 2013; Act A, 1999; Auerbach and Ruff, 2006)

Yet, the question is to which degree the normal facial asymmetry affects the mirroring concept in virtual craniomaxillofacial reconstruction. Therefore this study was conducted to determine the degree of asymmetry between right and left halves of the mandible.

Materials and methods:

The study included a total of 21 facial CT scans of patients attended Nasser Institute Hospital complaining of midfacial trauma All 21 subjects had intact mandible and a normal maxillofacial skeletal pattern. Inclusion criteria were set as follows: 1) age, not less than 18 years, 2) no previous mandibular surgery, 3) no congenital deformities, and 4) normal tempromanidular joint.

CT scan and data acquisition:

In each case, a preoperative computed tomography (CT) scan was performed (slice thickness, 0.5 mm; Aquilion 64 computed tomograph, Toshiba, Japan,). The scan data were imported as Digital Imaging and Communications in Medicine (DICOM) standard files for use with surgical simulation software.

Based on data obtained from the surgical simulation software, 3D virtual mandible models were reconstructed. Each mandible was splitted into two halves. On each half eight points were marked for 3D linear and angular measurements, these measurements were adopted from **Lin et al. (2014)** study. Another nine points were selected on the whole mandible at its bottom view. All these points are listed in tables (1) and figure (1). After marking of these points, 3D linear and angular which were recorded, and listed in table (2) and (3), and shown in figure (2) and (3) respectively. 2D measurements also were taken to differentiate between the buccolingual thickness of right and left halves of the mandible. Points for measurements of buccolingual thickness were first marked at 3D model, and then had been measured at the 2D axial cut. These points were taken at 3 levels, level**1** (Th_a) at the alveolar bone level, level **2** (Th_b) at level just above mental nerve midway between level **1** and level **3**, and level 3 (Th_c) is at the inferior border. 3 points were taken at each level on each side. These points are listed in table (4), and shown in figure (4). All points were registered independently by the three authors then the mean of each variable was used for statistical analysis.

Statistical of analysis:

Analysis of data was performed using SPSS 17 (Statistical Package for Social Studies) for Windows.

Description of analysis:

Description of quantitative variables was registered in the form of mean, standard deviation (SD). Data were explored for normality using Kolmogorov-Smirnov test of normality. Since most of data were normally distributed, paired Student's ***t*** test was used for the comparisons between the right and left halves.

Results were expressed in the form p-values that were differentiated into:

* Non-significant when p-value > 0.05

* Significant when p-value ≤ 0.05

RESULT

Patients' age:

The age of patients ranged from 18 to 55 years, with a mean 32.33±12.23 yrs.

I- 2 D measurements

a. Comparing the right and left sides, revealed a non-significant difference in all measurements, except for Th_{b1} and Th_{c1} values (Table 5, Figure 5). The greatest mean difference between the right, left side was recorded in Th_{b1}, while the least mean difference was recorded in Th_{b3} (Table 5, Figure.6)

II- 3 D measurements

Comparing the right and left sides, revealed a non-significant difference in all linear and angular measurements (Table 6, Figure.7and 8). The greatest mean difference between the right, left side was recorded in angular measurement M13, while the least mean difference was recorded in the angular measurement M14 (Table 6, Figure.9).

Table (1).

Definition of landmarks and planes that were marked on virtual 3D mandible for 3D linear and angular measurements of the mandible.

Landmarks	Definition
L1	The most inferior point of the anterior part of mandibular body.
L2	The most inferior point of the posterior part of mandibular body.
L3	The most protruding point of the posterior margin of mandibular body.
L4	The most concave point of the posterior edge of mandibular ramus.
L5	The most protruding point of the posterior margin of mandibular condyle.
L6	The most protruding point of the top margin of mandibular condyle
L7	The most protruding point of the anterior margin of mandibular coronoid process.
L8	The most concave point of the anterior margin of mandibular ramus
L9	point at the inferior border of the mandible at the midline
L10	point at the inferior border of the mandible below the inferior border of canine at right side
L11	point at the inferior border of the mandible below the inferior border of canine at left side
L12	Point at the widest area at the inferior border of the mandible at its bottom view at right side
L13	Point at the widest area at the inferior border of the mandible at its bottom view at left side
L14	The most medial point at the condylar head at bottom view of the mandible at right side
L15	The most medial point at the condylar head at bottom view of the mandible at left side
L16	The most lateral point at the condylar head at bottom view of the mandible at right side
L17	The most lateral point at the condylar head at bottom view of the mandible at left side **Planes:**
Pa	The plane of the posterior margin of ramus formed by landmarks L3, L5 left and right side
Pb	The plane of the inferior margin of corpus formed by landmarksL1, L2 of left and right side
Pc	Mid sagittal plane

Table (2).
3D linear measurements of the mandible.

Measurement	Definition
M1	The minimum distance between concave point of anterior edge of mandibular ramus (L8) and concave point of mandibular ramus flexure (L4).
M2	The maximum distance between convex point of anterior edge of mandibular coronoid process (L7) and posterior point of mandibular condyle (L5).
M3	Distance between posterior point of mandibular condyle (L5) and concave point of mandibular ramus flexure (L4).
M4	Distance between posterior protruding point of mandibular corpus (L3) and concave point of mandibular ramus flexure (L4).
M5	Vertical distance from concave point of mandibular ramus flexure (L4) to posterior plane of mandibular ramus (Pa).
M6	Vertical distance from concave point of mandibular ramus flexure (L4) to bottom plane of the mandibular body (Pb).
M7	Vertical distance from highest point of mandibular condyle (L6) to bottom plane of the mandibular body (Pb).
M8	Vertical distance between mandibular ramus vertical height (M7) and mandibular ramus flexure vertical height (M6).
M9	Vertical distance between the most medial point (L14)at right side and (L15) at left side to the midsagittal plane.

Table (3)
3D angular measurements of the mandible.

Measurement	Definition
M10	Angle formed by the posterior plane of mandibular ramus (Pa) and the bottom plane of the mandibular body (Pb).
M11	The intersecting angle between mandibular flexure upper border (M3) and the plane parallel to the bottom plane of the Mandibular body (Pa).
M12	Angle formed by mandibular flexure upper border (M3) and mandibular flexure lower border (M4).
M13	Angle formed by connecting 3 points L9, L10, and L12 at right side. L9, L11, and L13 at the left side
M14	Angle formed by midsagittal plane (pc) and a line connectingL14and L16at right side. L15 and L17 at left side

Table (4).
Definition of 2D landmarks that were first marked on 3D then measured at 2D axial cut

landmark	definition
Th_{a1}	point at the alveolar bone level at the retromolar area on the external oblique ridge
Th_{a2}	point at the alveolar bone level between 1st and 2nd premolar
Th_{a3}	point at the alveolar bone level on the buccal bone of the canine
Th_{b1}	Point at level just above mental nerve midway between level 1 and level 3 at the retromolar area on the external oblique ridge
Th_{b2}	Point at level just above mental nerve midway between level 1 and level 3 between 1st and 2nd premolar
Th_{b3}	Point at level just above mental nerve midway between level 1 and level 3 on the buccal bone of the canine
Th_{c1}	Point at the inferior border at the retromolar area on the external oblique ridge
Th_{c2}	Point at the inferior border between 1st and 2nd premolar

Th_{c3}	Point at the inferior border on the buccal bone of the canine

Table (5)

Mean standard deviations and mean difference of 2 D measurements in right, left side and significance of difference (paired Student's *t* test)

	Right		Left		Difference		t value	P value
	Mean	SD	Mean	SD	Mean	SD		
Th_{a1}	11.93	1.82	11.83	1.91	1.029	0.743	0.356	0.725^{ns}
Th_{a2}	9.23	1.57	8.95	1.63	0.98	0.78	1.060	0.103^{ns}
Th_{a3}	11.31	1.84	11.25	1.85	0.64	0.48	0.293	0.772^{ns}
Th_{b1}	9.37	1.98	8.59	1.82	1.24	0.63	3.055	0.006^{s}
Th_{b2}	9.70	2.04	9.70	2.00	0.84	0.48	0.038	0.97^{ns}
Th_{b3}	9.75	2.19	9.82	1.99	0.63	0.48	0.38	0.706^{ns}
Th_{c1}	7.08	1.82	6.54	1.62	0.84	0.54	2.92	0.008^{s}
Th_{c2}	8.74	1.30	8.50	0.96	0.81	0.56	1.124	0.274^{ns}
Th_{c3}	9.35	1.46	9.49	1.83	0.82	0.36	0.599	0.555^{ns}

Table (6)

Mean standard deviations and mean difference of 3 D measurements in right, left side and significance of difference (paired Student's *t* test)

		Right		Left		Difference		*t* value	P value
		Mean	SD	Mean	SD	Mean	SD		
Linear	M1	35.05	4.30	35.48	4.12	1.57	0.87	1.105	0.282^{ns}
	M2	45.86	5.34	45.90	5.58	1.86	1.42	0.0918	0.928^{ns}
	M3	28.05	6.28	26.93	6.09	3.07	3.17	1.188	0.248^{ns}
	M4	15.88	5.10	15.86	3.98	3.02	2.11	0.029	0.977^{ns}
	M5	2.52	0.98	2.33	0.80	0.52	0.51	1.022	0.237^{ns}
	M6	29.33	7.15	30.48	7.64	3.71	2.76	1.15	0.264^{ns}
	M7	64.24	10.16	64.52	10.01	2.38	2.42	0.832	0.706^{ns}
	M8	34.90	6.84	33.62	6.65	2.81	2.46	1.659	0.112^{ns}
	M9	39.86	5.82	38.95	6.26	0.91	2.84	1.46	0.160^{ns}
Angular	M10	119.40	6.53	119.29	6.57	2.31	1.90	0.18	0.859^{ns}
	M11	56.24	5.94	55.62	6.56	3.43	2.81	0.673	0.531^{ns}
	M12	166.31	5.44	166.81	4.55	3.83	3.84	0.419	0.68^{ns}
	M13	145.95	12.10	146.29	10.73	3.86	3.32	0.296	0.77^{ns}
	M14	69.81	7.55	69.67	8.34	0.143	7.28	0.089	0.929^{ns}

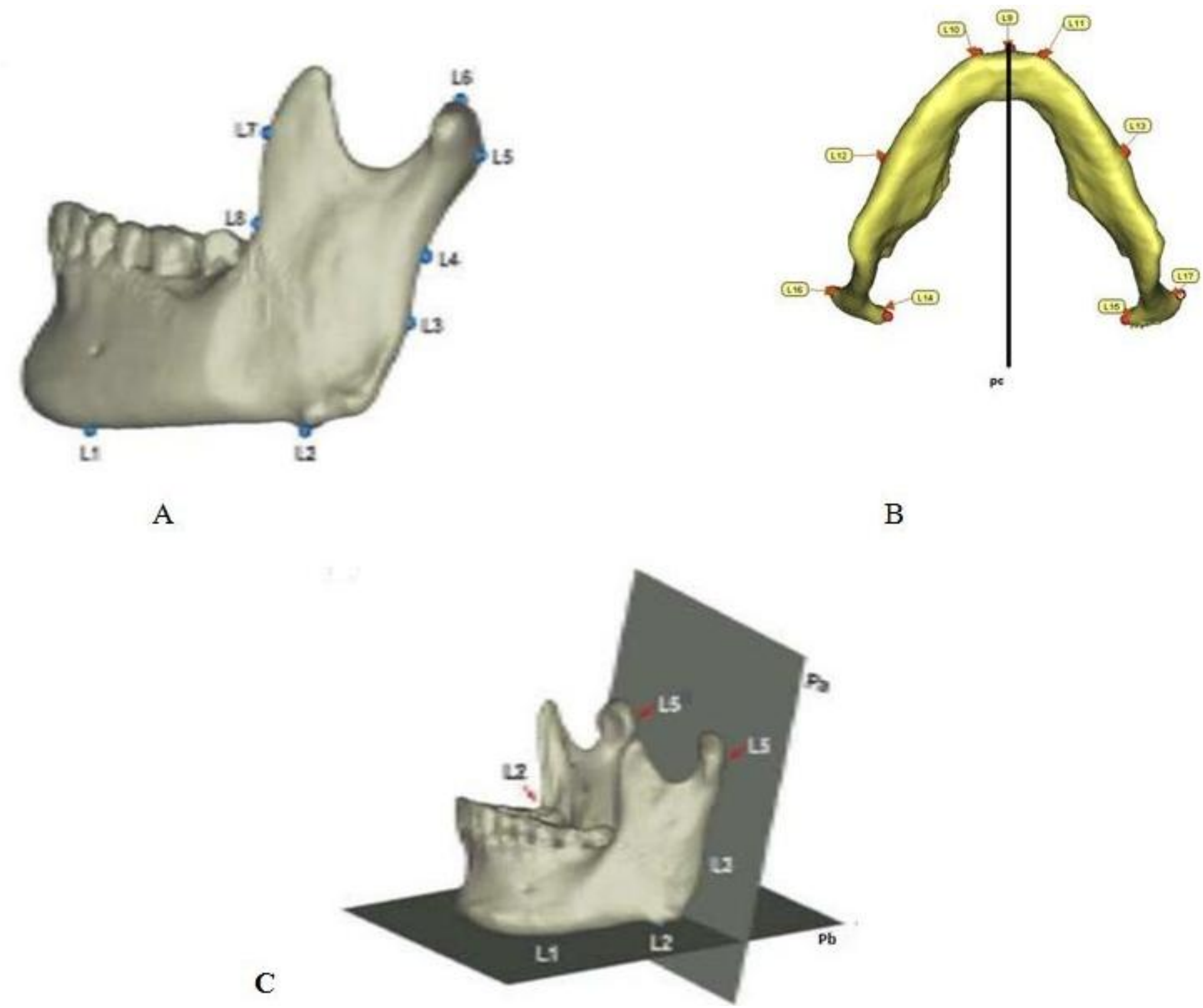

Fig. (1). Definition of landmarks and planes that were marked on virtual 3D mandible.
For 3D linear and angular measurements of the mandible**,(A). L1**. The most inferior point of the anterior part of Mandibular body; **L2**. The most inferior point of the posterior part of mandibular body; **L3**. The most protruding point of the posterior margin of mandibular body; **L4**. The most concave point of the posterior edge of mandibular ramus. **L 5**; the most protruding point of the posterior margin of mandibular condyle; **L6**. The most protruding point of the top margin of mandibular condyle; **L7**. The most protruding point of the anterior margin of mandibular coronoid process; **L8**. The most concave point of the anterior margin of mandibular ramus. **(B). L9**. Point at the inferior border of the mandible at the midline**; L10**. Point at the inferior border of the mandible below the inferior border of canine at right side; **L11**. Point at the inferior border of the mandible below the inferior border of canine at left side; **L12**. Point at the widest area at the inferior border of the mandible at its bottom view at right side; **L13**. Point at the widest area at the inferior border of the mandible at its bottom view at left side; **L14**. The most medial point at the condylar head at bottom view of the mandible at right side; **L15**. The most medial point at the condylar head at bottom view of the mandible at left side; **L16**. The most lateral point at the condylar head at bottom view of the mandible at right side; **L17**. The most lateral point at the condylar head at bottom view of the mandible at left side. **(C)**.Planes: **Pa**. The plane of the posterior margin of ramus formed by landmarks L3, L5 left and right side; **Pb**. The plane of the inferior margin of the body formed by landmarks L1, L2 of left and right side; **Pc**. The midsagittal plane of the mandible.

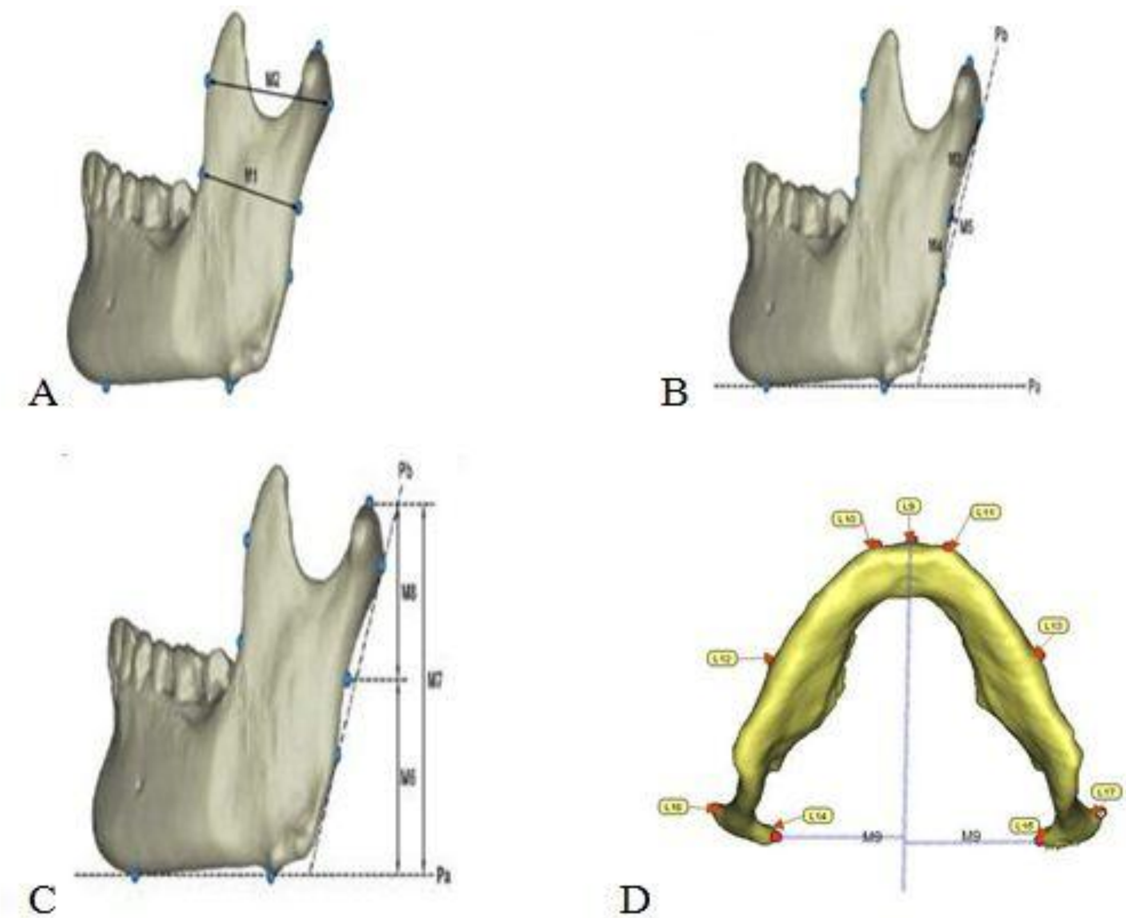

Fig. (2).Definition of 3D linear measurement of the mandible.

(**A), M**; the minimum distance between concave point of anterior edge of mandibular ramus (L8) and concave point of mandibular ramus flexure (L4). **M2**; the maximum distance between convex point of anterior edge of mandibular coronoid process (L7) and posterior point of mandibular condyle (L5**). (B)**, **M3**; distance between posterior point of mandibular condyle (L5) and concave point of mandibular ramus flexure (L4). M4, distance between posterior protruding point of mandibular body (L3) and concave point of mandibular ramus flexure (L4).M5, vertical distance from concave point of mandibular ramus flexure (L4) to posterior plane of mandibular ramus (Pa).**(C), M6**; vertical distance from concave point of mandibular ramus flexure (L4) to bottom plane of the mandibular body (Pb). **M7**; vertical distance from highest point of mandibular condyle (L6) to bottom plane of the mandibular body (Pb).**M8**; vertical distance between mandibular ramus vertical height (M7) and mandibular ramus flexure vertical height (M6).**(D), M9**; vertical distance between the most medial point (L14) at right side and (L15) at left side to the midsagittal plane.

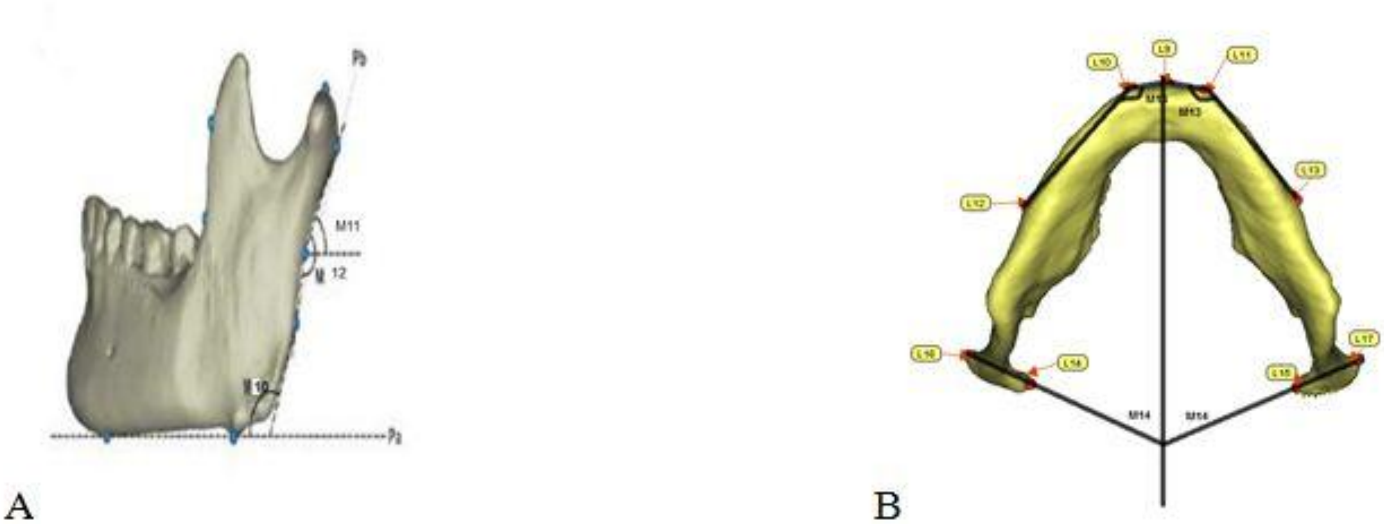

Fig. (3). 3D angular measurements of the mandible.
M10. Angle formed by the posterior plane of mandibular ramus (Pa) and the bottom plane of the mandibular body (Pb), **(A)**; **M11**. The intersecting angle between mandibular flexure upper border (M3) and the plane parallel to the bottom plane of the mandibular body (Pa). **M12**. Angle formed by mandibular flexure upper border (M3) and mandibular flexure lower border (M4), **(B)**. **M13**. Angle formed by connecting 3 points L9, L10, and L12 at right side. L9, L11, and L13 at the left side; **M14**. Angle formed by midsagittal plane (pc) and a line connectingL14 and L16at right side, L15 and L17 at left side.

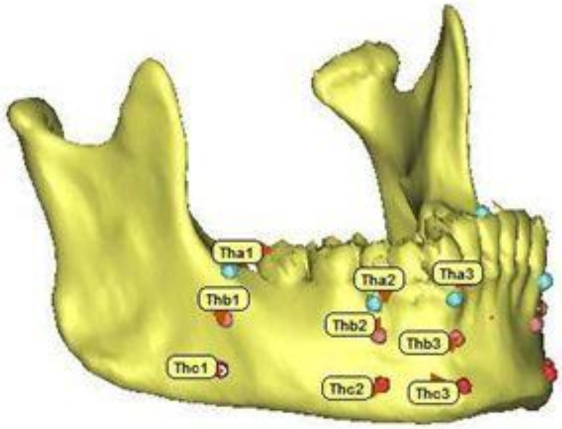

A

C

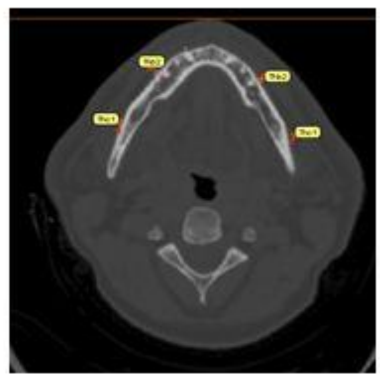

B

Fig. (4). Definition of 2D landmarks.

Definition of 2D landmarks, which were first marked on 3D **(A),** then measured at 2D axial cut (**B** and **C**); **Th_{a1}**. Point at the alveolar bone level at the retromolar area on the external oblique ridge;**Th_{a2}**. Point at the alveolar bone level between 1st and 2nd premolar;**Th_{a3}**. Point at the alveolar bone level on the buccal bone of the canine.**Th_{b1};** point at level just above mental nerve midway between level 1 and level 3 at the retromolar area on the external oblique ridge; **Th_{b2}**. Point at level just above mental nerve midway between level 1 and level 3 between 1st and 2nd premolar;**Th_{b3}**. Point at level just above mental nerve midway between level 1 and level 3 on the buccal bone of the canine; **Th_{c1}**. Point at the inferior border at the retromolar area on the external oblique ridge; **Th_{c2}.** Point at the inferior border between 1st and 2nd premolar; **Th_{c3}**. Point at the inferior border on the buccal bone of the canine.

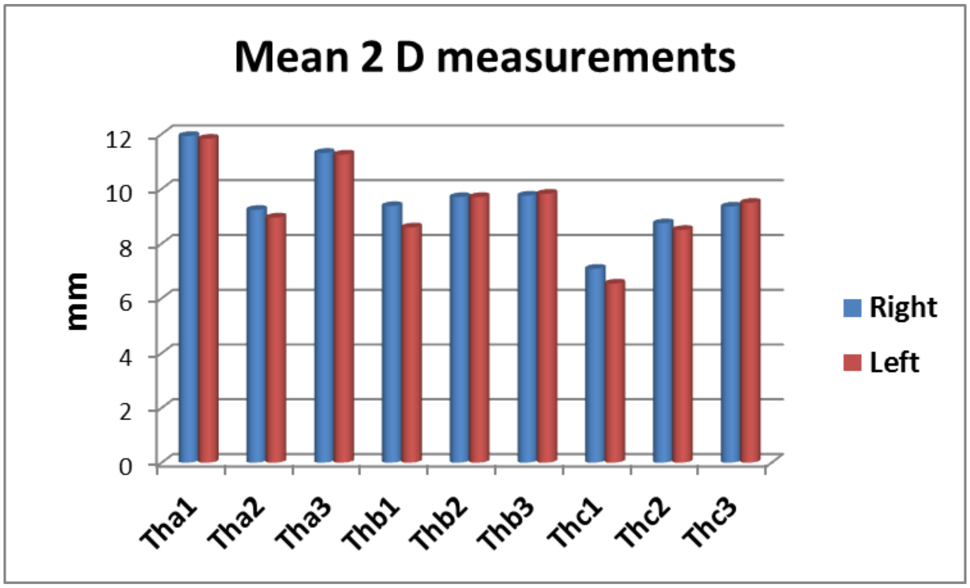

Fig. (5). Column chart showing mean values of 2 D measurements (mm) in right, left side.

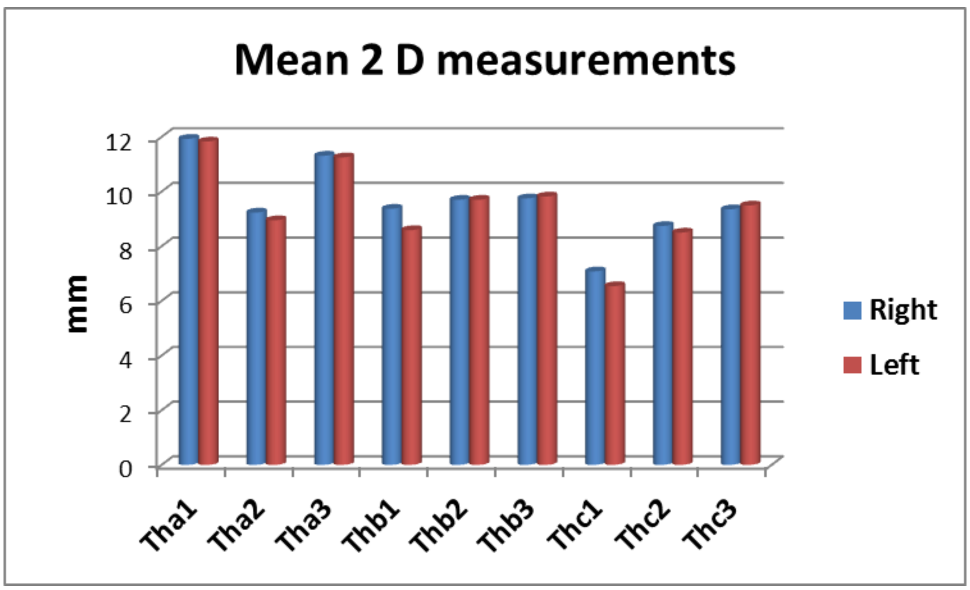

Fig. (6). Column chart showing mean difference of 2 D measurements (mm) in right, left side.

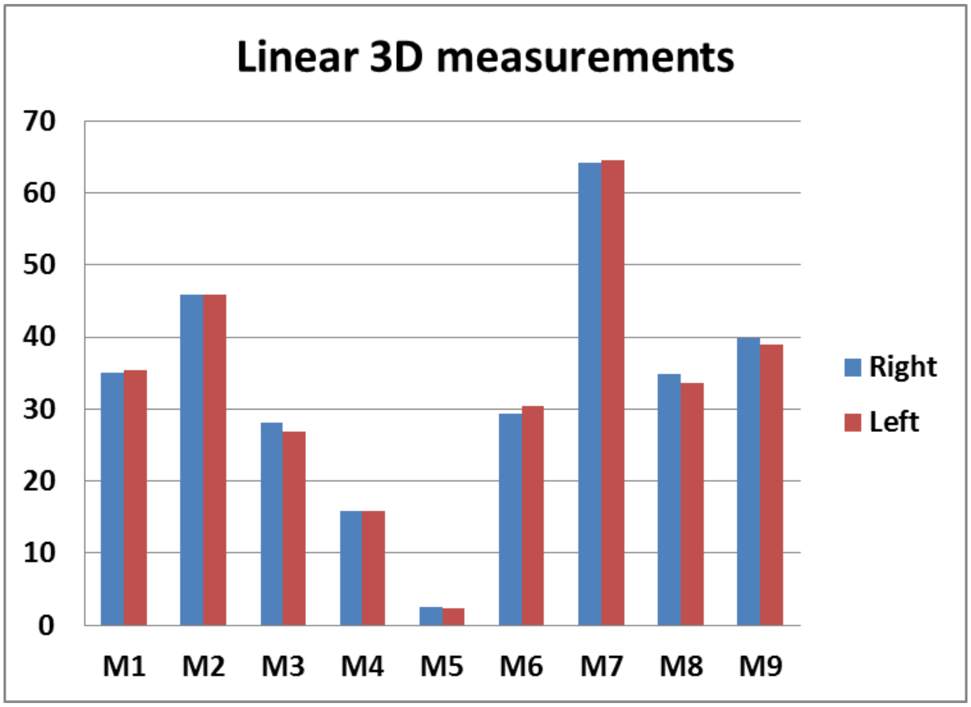

Fig. (7). Column chart showing mean values of linear 3 D measurements (mm) in right, left side.

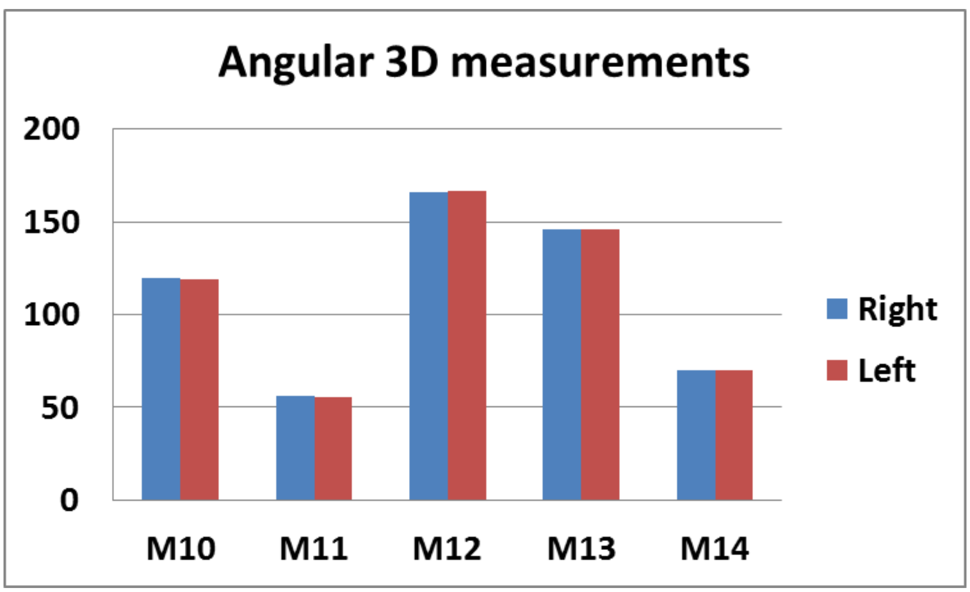

Fig. (8). Column chart showing mean values of angular 3 D measurements in right, left side.

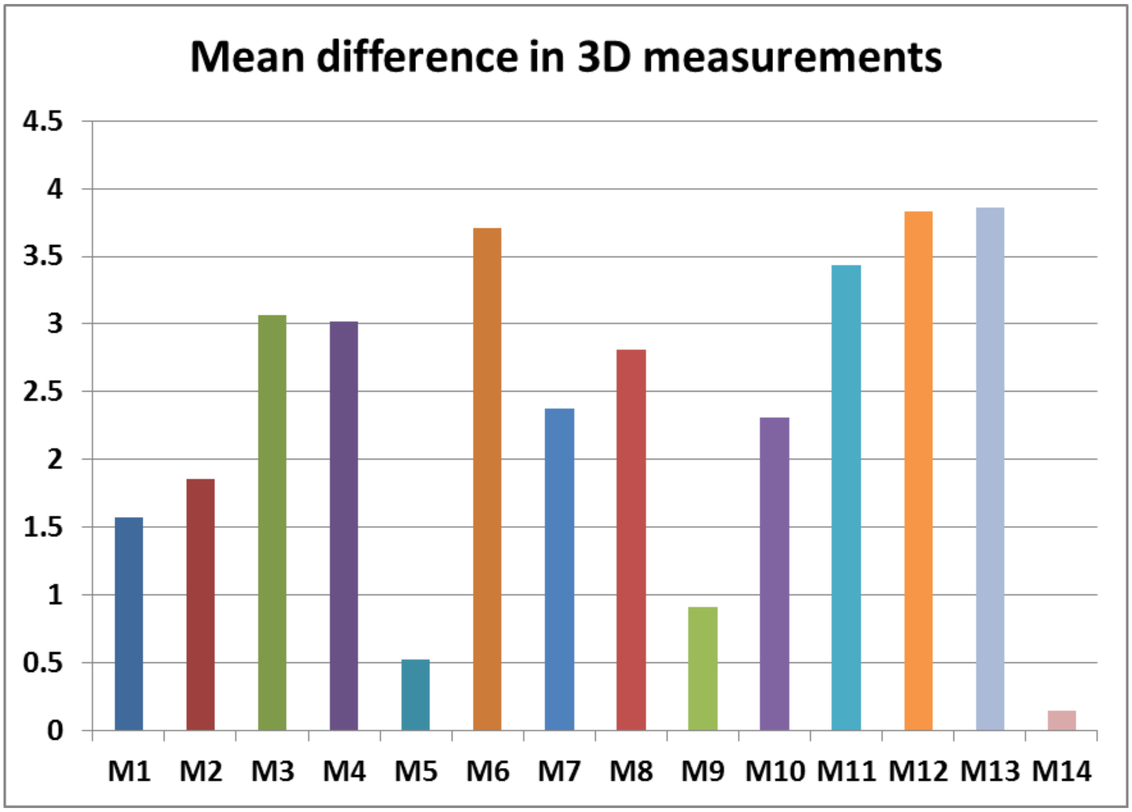

Fig. (9) Column chart showing mean difference of 3 D measurements in right, left side

Discussion

This study was undertaken trying to answer the question if the right side of the mandible can replace the left side and vice versa in case of unilateral large mandibular defect and hemimandiblectomy using mirroring tool without any other adjustments.

The aim of operation planning in oral and maxillofacial surgery is an optimization of the surgical result to restore function, form, and the esthetic appearance, which is to a certain degree depends on obtaining facial symmetry. To restore facial symmetry, a standard procedure for preoperative planning is performed using the mirroring tool for unilateral defects, reconstructing the asymmetric portion, using its normal counterpart working as a reference template. Nevertheless, comparing the preoperative planning by mirroring of the unaffected side to the affected one with surgical outcome, verified that the accuracy of this approach could be influenced by the presence of natural asymmetry of the skulls. (Benazzi and Sneck, 2011)

It has been well recognized that asymmetry characterizes human paired and unpaired skeletal segments. In regard to the skull, in particular, facial bones, the more asymmetric the shape, the less reliable is the definition of the mid-sagittal plane, which is essential for mirroring procedures. Accordingly, mirroring the unaffected side in almost symmetric skulls/faces could be a proper solution for bone reconstruction. But for more asymmetric skulls/faces, other solutions would be required. **Lee et al. (2007)** maintained the condylar cap of the affected side in virtual reconstruction of the mandible after hemimandiblectomy rather than complete mirroring of the normal side, this condylar cap used as a guide-post to insure accurate positioning of the final construct.

Benazzi and Senck (2011) had described three methods of virtual reconstruction of digital osteotomized zygomatic bone on 15 skulls using different types of surgical simulation software. They found some skulls have low degree of asymmetry, thus mirroring the unaffected side with the affected one allowed restoration of the missing part without attempting any manual alignment of the reflected part onto the affected one. The second group in which the mirrored hemiface was aligned to the affected side using iterative closest points, accordingly, the missing part was replaced by the bone segment of the aligned normal mirrored hemiface with some degree of manual alignment. In the third, the mirrored cranium was warped onto the original one by applying the thin plate spline (TPS) algorithm.

In this study, anthropometric measurements were used on virtual 3D and 2D axial cuts to determine the degree of difference between right and left halves of the mandible.

Using paired Student's *t* test, to analyze the difference between right and left halves of the mandible. Regarding 2D linear measurements of right and left halves revealed a non- significant difference in buccolingual dimensions between right and left halves except at the region just above the mental nerve and on the external oblique ridge (Th_{b1}) and at the inferior border at the retromolar area (Th_{c1}).Comparing 3D linear and angular measurements of right and left halves revealed a non- significant difference, in all variables.

These results coincide with the result of **Lin et al. (2014)** study that found no statistical significance between right and left halves of the mandible. The results also work in accordance with the results of **Park et al. (2014)** study of the measurements of the mandibular ramus thickness as they found no statistical significant difference between right and left halves.

Conclusion

The findings of this study revealed that the mirroring tool is a reliable method in virtual reconstruction of the mandible in cases of unilateral mandibular defect and hemimandiblectomy with subsequent printing STL model for preoperative adaptation of the reconstruction plate

Reference

Albert A. M, Greene D.L. (1999): Bilateral Asymmetry in Skeletal Growth and Maturation as an Indicator of Environmental Stress. Am J PhysAnthropol. 110:341-349

Auerbach BM, Ruff CB. (2006): Limb bone bilateral asymmetry: variability and commonality among modern humans. J Hum Evol. 50(2):203-18.

Benazzi S, Senck S. (2011): Comparing 3-dimensional virtual methods for reconstruction in craniomaxillofacial surgery. J Oral Maxillofac Surg. 69(4):1184-94.

Bigoni L, Krajíček V, Sládek V, Velemínský P, Velemínská J. (2013): Skull shape asymmetry and the socioeconomic structure of an early medieval central European society. Am J PhysAnthropol. 150(3):349-64.

Edwards SP. (2010): Computer-assisted craniomaxillofacial surgery. Oral MaxillofacSurgClin North Am. 22(1):117-34.

Gawlikowska a, Szczurowski J, Czerwiński F, Miklaszewska D, Adamiec E, Dzieciołowska E. (2007): The fluctuating asymmetry of medieval and modern human skulls. Homo. 58(2):159-72.

Lee J-W, Fang J-J, Chang L-R, Yu C-K. (2007): Mandibular defect reconstruction with the help of mirror imaging coupled with laser stereolithographic modeling technique. J Formos Med Assoc. 106(3):244-50.

Lin C, Jiao B, Liu S, Guan F, Chung N-E ,Han S-H, Lee U-Y. (2014): Sex determination from the mandibular ramus flexure of Koreans by discrimination function analysis using three-dimensional mandible models. Forensic Sci Int. 236:191.e1-6.

Markiewicz MR, Bell RB. (2011): The use of 3D imaging tools in facial plastic surgery. Facial PlastSurgClin North Am. 19(4):655-82.

Modabber A, Gerressen M, Stromps J, Riediger D, Hölzle F, Ghassemi A. (2013): Computer-assisted zygoma reconstruction with vascularized iliac crest bone graft. Int J Med Robotics Comput Assist Surg. 9: 497–502.

Park K-R, Kim S-Y, Kim G-J, Park H-S, Jung Y-S. (2014): Anatomic study to determine a safe surgical reference point for mandibular ramus osteotomy. J Craniomaxillofac Surg. 42(1):22-7.

Pirgousis P, Brown D, Fernandes R. (2013): Digital measurements of 120 mandibular angles to determine the ideal fibula wedge osteotomy to re-create the mandibular angle for microvascular reconstruction. J Oral Maxillofac Surg. 71(12):2169-75.

Rahimov C, Farzaliyev I. (2011): Virtual bending of titanium reconstructive plates for mandibular defect bridging: review of three clinical cases. Craniomaxillofac Trauma Reconstr. 4(4):223-34.

Salgueiro MI, Stevens MR. (2010): Experience with the use of prebent plates for the reconstruction of mandibular defects. Craniomaxillofac Trauma Reconstr. 3(4):201-8.

Yamada H, Ishihama K, Yasuda K,Nakayama H.Y, kayama M, Yamada T, Furusawa K. (2010): Precontoured mandibular plate with three-dimensional model significantly shortened the mandibular reconstruction time. Asian J Oral Maxillofac Surg. 22(4):198-201.

Zhao L, Patel PK, Cohen M. (2012): Application of virtual surgical planning with computer assisted design and manufacturing technology to cranio-maxillofacial surgery. Arch Plast Surg. 39(4):309-16.